Macromolecules

pubs.acs.org/Macromolecules Article

Red Sea Star-Inspired, Rapid Underwater Self-Healing Polyurethane Based on Dual Hydrophobic Units and Tandem Dynamic Bonds

Fenglong Li, Haofeng Qiu, Chao Chen, Xiaolin Wang, Minghui Cui, Shijie Qiu, Kyung Jin Lee, Jing Chen,* Wu Bin Ying,* and Jin Zhu

Cite This: *Macromolecules* 2025, 58, 5019−5028 Read Online

ACCESS | Metrics & More | Article Recommendations | Supporting Information

ABSTRACT: Red sea stars exhibit an extraordinary underwater self-healing capability driven by fibrinolytic enzyme secretion, enabling survival in challenging marine environments. Inspired by this biological mechanism, we developed a polyurethane (DSFPU-3) capable of rapid underwater self-healing. By integrating dual hydrophobic units (alkyl side chains and fluorine groups) with tandem dynamic bonds (disulfide and imine bonds), DSFPU-3 achieved a water contact angle of 99.3° and maintained stable microphase structures and micromorphology even after 4-day water soaking. The synergistic effect of hydrophobic units and dynamic bonds enabled self-healing at a speed exceeding 33.33 μm/h, achieving 98% efficiency and allowing the material to endure significant mechanical stress post-healing. Small-molecule modeling experiments and rheological analyses validated the bond exchange mechanisms of the tandem dynamic bonds, underscoring their critical role in accelerating the self-healing process. This study presents a novel strategy for fabricating rapid underwater self-healing polyurethanes, representing a significant advancement in their application under aquatic conditions.

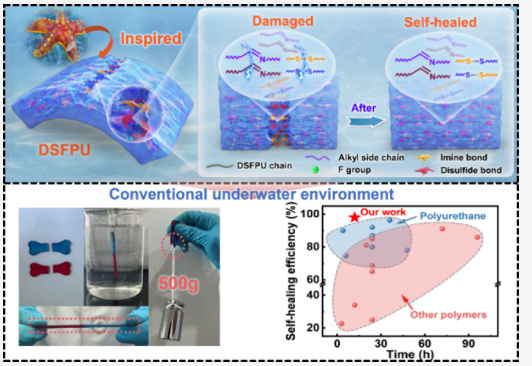

1. INTRODUCTION

In recent years, self-healing materials have attracted increasing interest from researchers.[1] By integrating self-healing abilities into materials, these materials can autonomously recover from structural and functional damage, thereby enhancing their lifespan, reliability, and durability.[2,3] Among various options, self-healing polyurethane stands out due to its versatility in structural design and ease of synthesis.[4] In studies of self-healing polyurethane, dynamic reversible covalent bonds were often introduced as the self-healing driving force, such as hydrogen bonds,[5,6] Diels−Alder reactions,[7−9] metal−ligand interactions,[10] disulfide metathesis,[11,12] and so on.[13−16] Unfortunately, room-temperature self-healing polyurethane faces challenges in meeting the requirements of wet or underwater environments,[17] such as those encountered in underwater robotics and implantable medical devices.[18] These challenges primarily arise because most of these dynamic bonds are unstable in water. When self-healing polyurethane contacts water molecules, these molecules can play various roles, such as donors and acceptors of hydrogen bonds, ligands, and polar solvents.[19] Water molecules may saturate hydrogen bonds, coordinate with metal cations, or solvate ions, significantly reducing the bonding stability. Consequently, dynamic bond exchange is disrupted by water molecules, resulting in a diminished self-healing capability. Therefore, compared to self-healing polyurethane designed for dry environments, there is an urgent need to develop polyurethane capable of underwater self-healing to meet the demands of aqueous environments.

Previous studies on underwater self-healing polyurethanes primarily employed two types of dynamic bonds: (i) boronic acid derivatives featuring boronic-ester or boroxine bonds[20] and (ii) hydrogen bonds formed between catechol groups inspired by mussels.[21] However, both approaches present limitations. Boronic acid derivatives are unstable underwater and prone to hydrolysis.[22] Catechol groups can interact closely in water, but the self-healing driving force is relatively weak.[23] To address these challenges, researchers have introduced hydrophobic polymer chains to protect dynamic bonds from the interference of water molecules, such as polydimethylsiloxane (PDMS),[24,25] polybutadiene (PB),[26] and poly(vinylidene fluoride-*co*-hexafluoropropylene).[27] Additionally, dynamic bonds are pivotal for enabling underwater self-healing. For instance, Kang et al. utilized bis(3-amino-propyl)-terminated PDMS as a hydrophobic soft segment, while employing 4,4′-methylene bis(phenyl isocyanate) (MDI) and isophorone diisocyanate (IPDI) as hard segments.[28] By introducing

Received: December 3, 2024
Revised: March 22, 2025
Accepted: April 16, 2025
Published: April 25, 2025

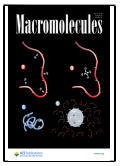

https://doi.org/10.1021/acs.macromol.4c03007
Macromolecules 2025, 58, 5019−5028

Scheme 1. (a) Red Sea Star Secretes Enzymes for Underwater Self-healing When Damaged, Which Contain Hydrogen Bonds and Dynamic Disulfide Bonds. (b) DSFPU Demonstrates Underwater Self-healing Capabilities, with Fluorine Groups and Alkyl Side Chains Preventing Water Molecule Interference, While Dynamic Disulfide Bonds and Imine Bonds Act as the Driving Forces for Underwater Self-healing

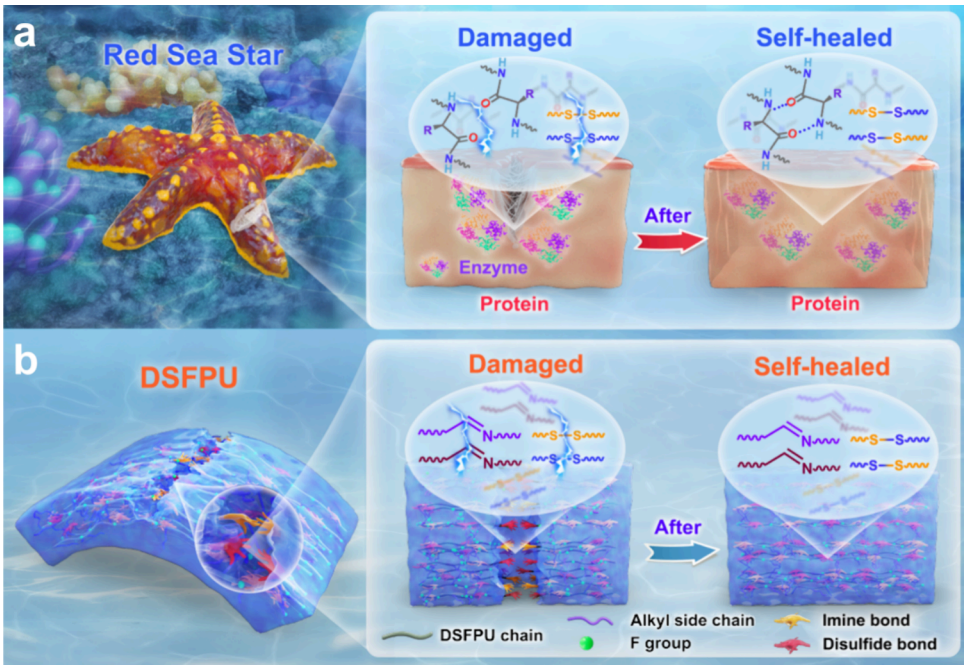

varying strengths of hydrogen bonds, a tough and underwater self-healing polyurethane was prepared that could completely self-heal after 72 h in water at room temperature. Similarly, Khatib et al. reported a highly water-insensitive self-healing polyurethane based on PB chains, disulfide bonds, and hydrogen bonds.[29] The polyurethane could autonomously self-heal at room temperature for 24 h, exhibiting a high self-healing efficiency (>80%) under underwater conditions. Although these studies have achieved underwater self-healing capabilities, challenges remain in optimizing the speed and efficiency of the process. Therefore, the key challenge we needed to address is the design of a polyurethane that can rapidly self-heal underwater at a conventional environment.

Marine invertebrates, especially echinoderms, possess remarkable underwater self-healing abilities, allowing them to autonomously repair damage and improve their chances of survival in aquatic environments.[30,31] The red sea star is a typical example of such marine self-healing. When injured, glands in its arms secrete fibrinolytic enzymes that facilitate the repair of damaged tissue.[32,33] These enzymes contain a high concentration of hydrogen bonds, disulfide bonds, and hydrophobic groups, enabling rapid underwater healing.[34] Inspired by the structure of these enzymes, we developed a polyurethane (DSFPU-3) with rapid underwater self-healing capability in a conventional environment. Polyester diols with alkyl side chains were selected as the soft segments, and fluorine groups were incorporated into the hard segment structure. The combination of alkyl side chains and fluorine groups provided dual hydrophobic protection from both the soft and hard segments. When submerged in water, DSFPU-3 could repel water molecules due to a dense hydrophobic barrier. Xu et al. proposed a strategy of dissociate transfer exchange (DTE) of tandem dynamic bonds.[35,36] The dissociation of disulfide bonds significantly enhanced the mobility of imine bonds in series with the breaking points, resulting in a rapid exchange rate and improved reprocessability. So, tandem disulfide and imine bonds were also incorporated as self-healing driving forces, enabling underwater self-healing through dual dynamic bond exchange without interference from water molecules. By optimizing the ratio of hydrophobic units to dynamic bond units, we aimed to develop a polyurethane with optimal underwater self-healing performance while exploring the synergistic mechanism of dual dynamic bonds under hydrophobic protection. This study introduces a novel strategy for creating underwater self-healing polyurethanes, advancing research and the application of underwater self-healing materials.

2. RESULTS AND DISCUSSION

The red sea star is a notable echinoderm recognized for its remarkable underwater self-healing abilities.[32] When the red sea star sustains unexpected damage, glands in its arms secrete fibrinolytic enzymes that facilitate the healing of the affected areas (Scheme 1a). These fibrinolytic enzymes contained an abundant number of hydrogen bonds, disulfide bonds, and hydrophobic groups, which enable the red sea star to achieve self-healing capabilities underwater. In specialized application scenarios, such as implantable biomedical devices, underwater sensors, and underwater robots, unexpected damage could compromise stability and reduce lifespan. Materials with underwater self-healing abilities could serve as effective solutions to these challenges. Inspired by the fibrinolytic enzymes secreted by the red sea star, we designed a functional polyurethane (DSFPU) aimed at replicating the exceptional underwater self-healing properties of this marine organism. DSFPUs were incorporated with dual hydrophobic units and tandem dynamic bonds (disulfide bonds and imine bonds), exhibiting self-healing capabilities underwater without external

https://doi.org/10.1021/acs.macromol.4c03007
Macromolecules 2025, 58, 5019−5028

stimuli. The low surface energy provided by fluorine groups and alkyl side chains, as shown in Scheme 1b, effectively prevents interference from water molecules. Furthermore, the dynamic exchange of tandem disulfide and imine bonds significantly enhances the underwater self-healing performance.

2.1. Small-Molecule Modeling to Elucidate Tandem Dynamic Bond Exchange. The fibrinolytic enzymes produced by the red sea star contain high levels of hydrogen bonds and disulfide bonds, which play a crucial role in enabling effective self-healing capabilities underwater. Inspired by this mechanism, we introduced tandem dynamic bonds into the polyurethane structure to increase dynamic bond exchange sites and improve the underwater self-healing performance. To validate this hypothesis, we conducted small molecular model experiments, synthesizing compounds containing only disulfide bonds, only imine bonds, and compounds with both disulfide and imine bonds, to investigate their dynamic exchange processes. As illustrated in Figure 1a, disulfide and imine bonds

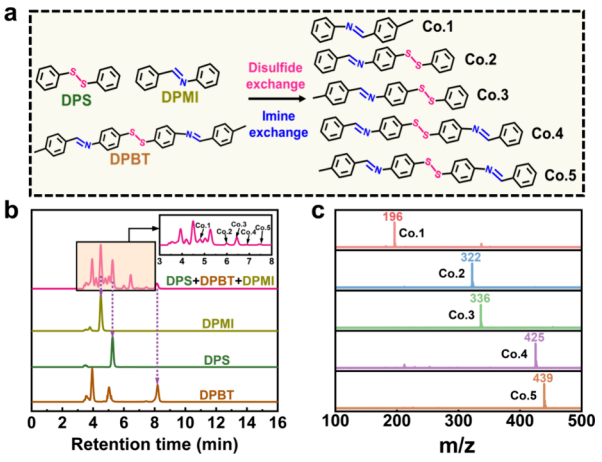

Figure 1. (a) Exchange mechanisms of imine bonds and disulfide bonds between DPS, DPMI, and DPBT. (b) LC-MS of DPBT, DPS, DPMI, and their mixtures. (c) Time-of-flight mass spectra of Co.1, Co.2, Co.3, Co.4, and Co.5.

could theoretically undergo simultaneous bond exchange, leading to the formation of various small molecular compounds. To examine these exchanges, we employed LC-Q-TOF to test the individual small molecules (DPS, DPBT, and DPMI) and their mixtures, discovering five new compounds in the mixture (Figure 1b). Figures 1c and S1 further validate the findings through time-of-flight mass spectra that, in addition to the three initial small molecular model compounds (DPMI, DPS, and DPBT), five other small molecules (Co.1, Co.2, Co.3, Co.4, and Co.5) were also detected. These results confirmed the exchange mechanism depicted in Figure 1a, demonstrating that bond exchange could occur simultaneously between disulfide bonds and imine bonds, providing a theoretical basis for the development of underwater self-healing polyurethanes.

2.2. Molecular Structure Design and Mechanical Properties. To create a polyurethane capable of self-healing underwater, introducing only tandem dynamic bonds as the self-healing driving force is insufficient. Since water molecules can influence the bond exchange and hinder underwater self-healing, incorporating hydrophobic units into the molecular structure is essential to shield against the interference of water molecules. We utilized a strategy combining dual hydrophobic units and tandem dynamic bonds to develop a rapid, underwater self-healing polyurethane. In this study, we synthesized the DSFPUs using a one-pot reaction, where polyester diol (PDG), chain extender with tandem dynamic bonds (SNOH), chain extender with fluorine groups (FOH), and isophorone diisocyanate (IPDI) were simultaneously added into the reactor within a glovebox to prevent water interference (Scheme 2). In detail, we employed ring-opening

Scheme 2. Schematic Illustration of the Synthesis of DSFPUs

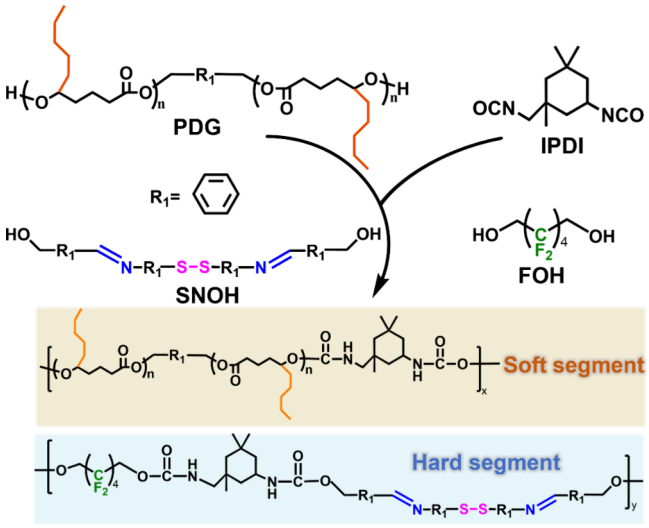

polymerization to prepare PDG with alkyl side chains as the soft segment, while the hard segment consisted of the designed chain extender with low-surface-energy fluorine groups and tandem dynamic bonds, along with IPDI. Five kinds of PUs (DSFPU-#) with different weight percentage ratios of [FOH]/[SNOH] were synthesized. The specific names were as follows: 3.4/0 (DSFPU-0), 2.55/0.85 (DSFPU-1), 1.7/1.7 (DSFPU-2), 0.85/2.55 (DSFPU-3), and 0/3.4 (DSFPU-4). The hydrophobic alkyl side chains and fluorine groups offered dual protection, minimizing the uniform distribution of water molecules within the polymer matrix and effectively reducing interference. Meanwhile, the tandem dynamic bonds served as the self-healing driving force, facilitating underwater self-healing. To enhance the underwater self-healing performance, we designed and synthesized a series of DSFPUs by adjusting the ratio of hydrophobic units to dynamic bond units. Detailed information on the design and synthesis methods can be found in the Experimental Section and Supplementary Table S1.

The ^{1}H NMR spectra confirmed the chemical structures of the target DSFPUs (Figure S2). Specifically, the peaks at 0.88 ppm (pillar 1) corresponded to the protons in the CH_3 units of PDG, the peaks near 1.09 ppm (pillar 2) could be attributed to CH_2 units in IPDI, the peaks at 4.58 ppm (pillar 3) belonged to protons in CH_2 units in FOH, and the peaks at 7.53 ppm (pillar 4) and 7.90 ppm (pillar 5) corresponded to the protons in the benzene ring of SNOH. Moreover, the areas of pillars 4 and 5 gradually increased with the contents of SNOH, indicating that the soft/hard segment ratio could be controlled as anticipated. Additionally, Figure 2a shows that the stretching vibration band at 2230 cm^{-1} corresponding to N═C═O disappeared, confirming the complete reaction of the -NCO groups. The stretching vibration bands at 1720 and 3350 cm^{-1}

https://doi.org/10.1021/acs.macromol.4c03007
Macromolecules 2025, 58, 5019−5028

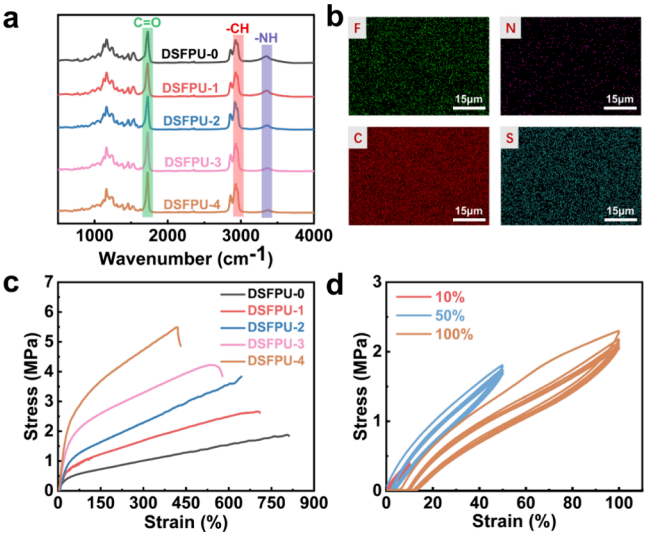

Figure 2. (a) Chemical structure of the DSFPUs. (b) FTIR spectrum of DSFPUs (DSFPU-0 ∼ 4) with various soft segment weight contents. (c) EDS images of DSFPU-3, containing elements C, N, S, and F. (d) Typical stress−strain curves of DSFPUs (DSFPU-0 ∼ 4) with the standard dumbbell specimen (ASTM D412). (e) Sequential cyclic tensile curves of DSFPU-3 at 10, 50, and 100% deformation were obtained five times.

further demonstrated the successful incorporation of PDG into the DSFPU molecular structure. As an example, the EDS image of DSFPU-3 in Figure 2b illustrates that the elements fluorine (F), nitrogen (N), carbon (C), and sulfur (S) were evenly distributed on the polyurethane surface. These results confirmed that the desired polyurethane was successfully synthesized according to the intended molecular structure. Additionally, the TGA and DTGA curves (Figure S3) indicated that the initial degradation temperatures of the DSFPUs exceeded 100 °C, demonstrating excellent thermal stability. The thermal stability improved with increasing SNOH content due to the aromatic rings in SNOH, which enhanced the overall thermal stability of DSFPU. The maximum decomposition temperature of DSFPU-0 was 285 °C, and with increased SNOH content, DSFPUs reached a maximum decomposition temperature of 328 °C, meeting the requirements for everyday use.

The typical stress−strain curves are shown in Figure 2c. Specifically, the tensile strength rose from 1.8 MPa for DSFPU-0 to 5.5 MPa for DSFPU-4, while the strain decreased from 811% for DSFPU-0 to 419% for DSFPU-4. This trend could be attributed to the increasing content of SNOH, which introduced a higher concentration of benzene rings in the polymer network. The rigid aromatic structures enhanced the physical cross-linking density, reinforcing the hard segment and leading to improved tensile strength. However, this also resulted in reduced chain mobility, limiting the material's ability to undergo large deformations, thereby decreasing elongation at break. Interestingly, the toughness of the DSFPUs initially increased and then decreased, as illustrated in Figure S4, with DSFPU-3 displaying the highest toughness of 17.9 MJ m^{-3}. The increased SNOH content in the hard segments promoted the formation of more hard-phase regions, which acted as anchor points, thereby gradually enhancing the toughness. DSFPU-3 exhibited an optimal ratio of soft to hard-phase regions, resulting in the highest toughness value. We further evaluated the elastic recovery performance of DSFPU-3 by subjecting it to cyclic stretching at strains of 10, 50, and 100% over five cycles. The cyclic stretching curves in Figure 2d indicated minimal hysteresis at a strain of 10%, with hysteresis beginning to appear as the strain increased. Even at a strain of 100%, DSFPU-3 maintained an elastic recovery rate of over 83%. This performance can be attributed to the microphase incompatibility between the soft and the hard phases of the polyurethane. This incompatibility leads to microphase separation, where the hard phase serves as an anchor for the soft phase, resulting in the high resilience of DSFPU-3.

2.3. Waterproof Properties of DSFPUs. For underwater self-healing materials to achieve optimal performance with minimal water interference, we introduced alkyl side chains and fluorine groups into the molecular structure to provide dual protection for both the soft and hard phases. By incorporating low-polarity polymer molecules, we restricted the penetration and uniform distribution of water molecules within the polymer matrix, thereby minimizing their disruptive influence and enhancing the effectiveness of underwater self-healing.[37] The results of the water contact angle tests in Figure 3a indicated that as the fluorine content decreased, the water contact angle of DSFPUs gradually decreased. DSFPU-0, having the highest fluorine content, exhibited the strongest hydrophobicity with a contact angle of 106.2°, while DSFPU-4 exhibited the lowest water contact angle at 95.4°. This variation was attributed to the proximity of shared electron pairs between carbon and fluorine atoms, which formed a

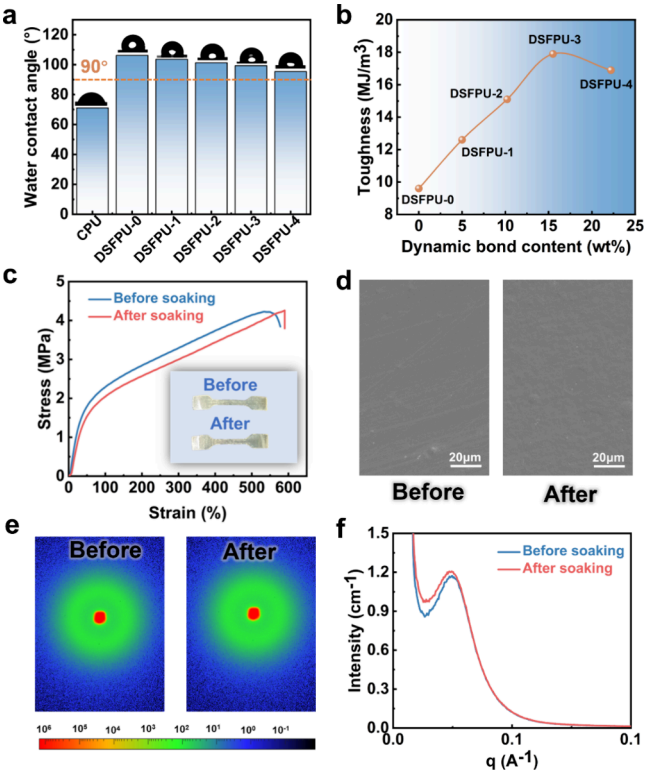

Figure 3. (a) Water contact angle of DSFPUs and commercial polyurethane. (b) Comparison of toughness and dynamic bond content of DSFPU. (c) Typical stress−strain curves of DSFPU-3 before and after soaking for 4 days. (d) SEM images of DSFPU-3 before and after soaking for 4 days represent changes in the micromorphology. (e) 2D-SAXS images and (f) 1D-SAXS curves of DSFPU-3 before and after soaking for 4 days represent changes in the microstructure after longtime water absorption.

https://doi.org/10.1021/acs.macromol.4c03007
Macromolecules 2025, 58, 5019−5028

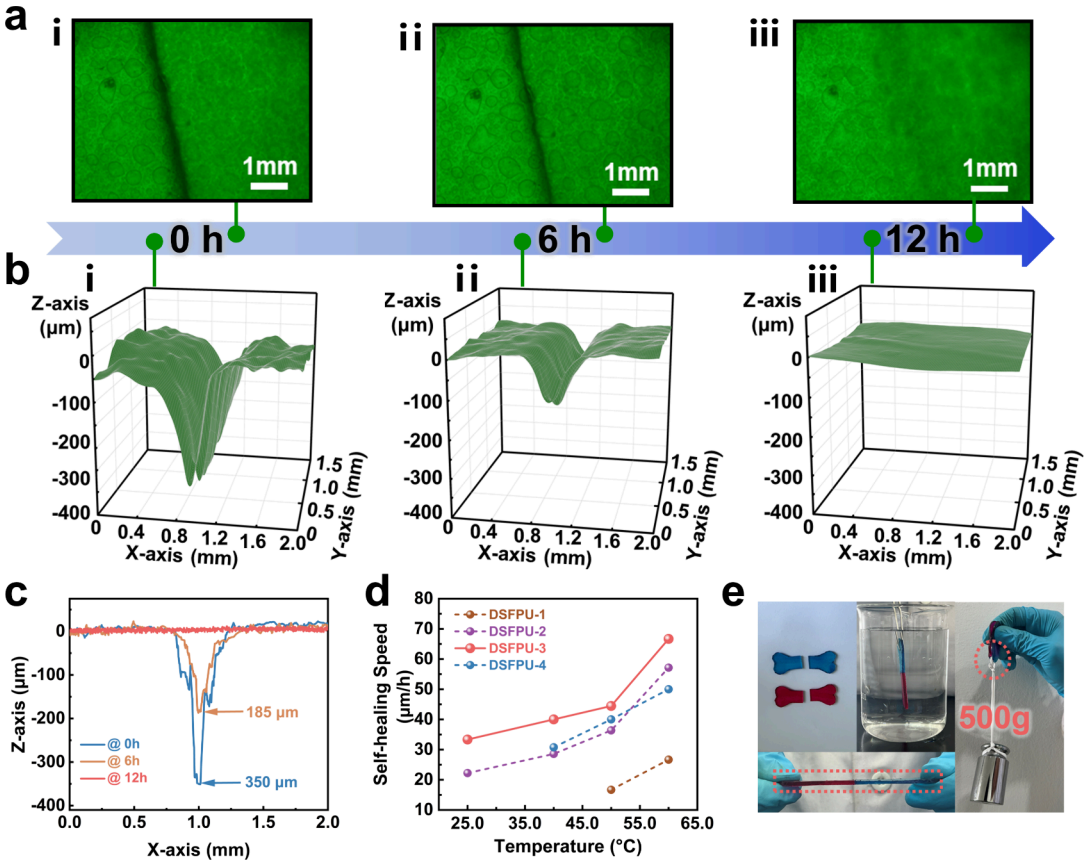

Figure 4. (a) Optical microscope images of the notched and self-healed DSFPU-3 film showing a gradual disappearance of the scar during underwater self-healing at conventional environment for 12 h. (b) Surface mapping microscopic images of a notched DSFPU-3 film at 0, 6, and 12 h at conventional environment. (c) Corresponding depth profiles of the notched DSFPU-3 during the underwater self-healing process in a conventional environment for 12 h. (d) Underwater self-healing speeds of notched DSFPU-3 at different temperatures calculated from [notch size]/[self-healing period]. (e) Images of the dyed DSFPU-3 film (~2 mm thickness) that was cut into two pieces, followed by the underwater self-healing in a conventional environment and subjected to a 500 g weight lifting test.

negatively charged protective layer, reducing surface energy and imparting distinctive hydrophobic properties to the fluorinated polyurethane. Therefore, under the same content of alkyl side chains, a higher fluorine content was correlated with improved hydrophobic performance. Furthermore, the DSFPUs were soaked in water, with contact angles and mass measured every 2 days to assess their water-proof properties. As shown in Figure S5, after 4 days of soaking, only DSFPU-4 exhibited a slight decrease in water contact angle, while the other polyurethanes remained virtually unchanged. Similarly, the mass of DSFPU-0 ~3 showed little change after 4 days of soaking, whereas DSFPU-4 exhibited a 3.5% increase in mass, which was consistent with the changes observed in the water contact angle (Figure S6). After a comprehensive assessment of the DSFPUs' toughness, dynamic bond content, and hydrophobic performance (Figure 3b), we selected DSFPU-3 for further testing. To assess the underwater puncture resistance of DSFPU-3, we conducted experiments using a common sharp object—a pencil. The results demonstrated that DSFPU-3 effectively resisted puncture without rupture (Figure S7). More importantly, thanks to its exceptional toughness, the punctured area of DSFPU-3 quickly returned to its original state after the test.

Water molecules have a significant negative effect on the mechanical properties of conventional self-healing materials. Upon accumulation within the polymer network, water molecules form hydrogen bonds with atoms in the network, such as nitrogen and oxygen. This accumulation reduces interactions between different polymer chains and acts as a plasticizer, ultimately leading to a decrease in mechanical properties and even causing degradation.[19] To assess the impact of water molecules on DSFPU-3's mechanical properties, we soaked it in water for 4 days. As shown in Figure 3c, the dumbbell-shaped sample of DSFPU-3 did not exhibit any whitening after soaking, and its mechanical properties remained virtually unchanged. Additionally, SEM was employed to observe the microstructure of DSFPU-3 before and after soaking. As illustrated in Figure 3d, the micromorphology remained unchanged, suggesting that water molecules had minimal impact on the microstructure. The aforementioned tests provided a macroscopic analysis of the hydrophobic performance of DSFPUs, while the microstructure played a critical role in determining their macroscopic properties. To further investigate the microphase structure of DSFPU-3 before and after soaking, we conducted SAXS analysis (Figure 3e). A circular scattering halo was observed in the DSFPU-3 sample before soaking, which was a characteristic feature of microphase separation between the soft and hard phases. After 4 days of soaking, the 2D SAXS image showed no noticeable changes. The nearly overlapping 1D integral intensity curves in Figure 3f, which align with the 2D SAXS image, further confirmed that the immersion did not

https://doi.org/10.1021/acs.macromol.4c03007
Macromolecules 2025, 58, 5019−5028

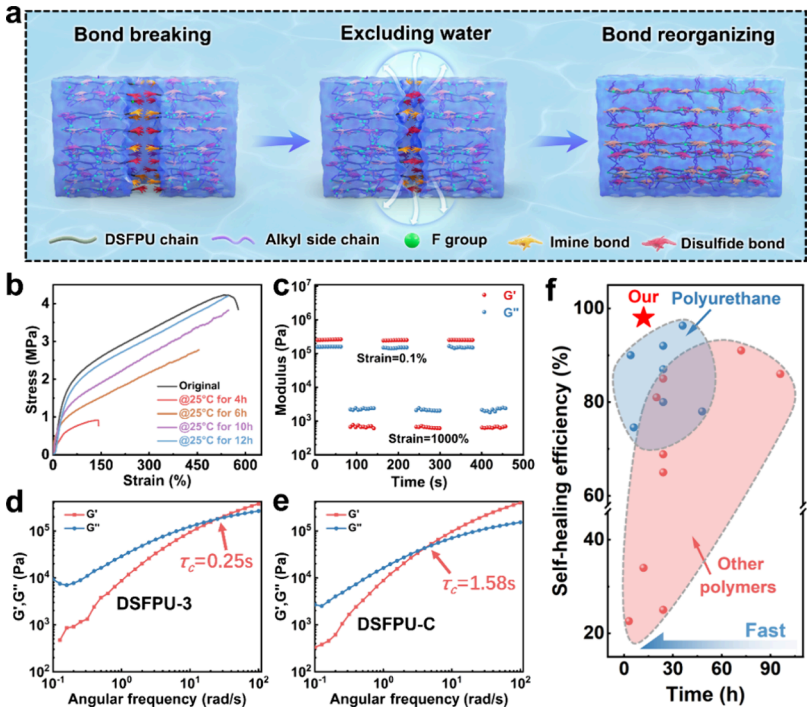

Figure 5. (a) Schematic diagram of the underwater self-healing process. (b) Stress−strain curves of the notched DSFPU-3 after self-healing in a conventional environment for different times. (c) Oscillatory time sweeps of DSFPU-3 tested using a rheometer with water in a conventional environment. Master curves (25 °C as a reference) of rheological results of (d) DSFPU-3 and (e) DSFPU-C (containing only dynamic disulfide bonds). (f) Comparison of the underwater self-healing time, and self-healing efficiency of DSFPU-3 with other polymers[18,24,43−49] (red) and polyurethan (blue).[29,50−54]

impact the microstructure of DSFPU-3. These tests validated the synergistic effect of alkyl side chains and fluorine groups in enhancing hydrophobic performance, establishing a fundamental basis for enabling underwater self-healing.

2.4. Rapid Underwater Self-Healing Properties of DSFPUs. To achieve underwater self-healing, we introduced alkyl side chains and fluorine groups into the molecular structure to provide dual protection for both the soft and hard phases, preventing water molecules from disrupting the self-healing process. Simultaneously, to enhance the underwater self-healing speed, we introduced tandem dynamic bonds (disulfide and imine bonds) to increase the frequency of dynamic bond exchange. Given that DSFPU-3 exhibited excellent mechanical properties, hydrophobicity, and a high content of dynamic bonds, we selected it for underwater self-healing experiments. A scratch was made in the center of the DSFPU-3 polyurethane film, and multiple drops of water were then applied to the scratch. The self-healing process was then observed under a polarizing microscope in a conventional environment. As shown in Figure 4a, the scratch gradually became less visible as healing progressed. After 12 h, the scratch had completely disappeared, indicating successful self-healing. To validate the contribution of hydrogen bonds to underwater self-healing, we replaced SNOH with BDO and synthesized a comparative polyurethane (DBFPU), as shown in Figures S8 and S9. The optical microscope images in Figure S10 indicated that hydrogen bonds did not make a significant contribution to the self-healing process underwater. The polarizing microscope provided a 2D view of the underwater self-healing process. Further observations were conducted by using a laser confocal microscope to capture a three-dimensional perspective of the scratch healing process. Figure 4b,c illustrates the results, demonstrating that as the underwater self-healing proceeded, both the width and depth of the scratch gradually decreased. Initially, the scratch had a depth of 350 μm; after 6 h of underwater self-healing, its depth reduced to 185 μm, and it was fully healed after 12 h, consistent with the observations from the polarizing microscope. In addition, to clarify the self-healing process, we tested the depth variation every 3 h to verify whether it follows an exponential decay pattern (Figure S11). The scratch depths at different healing times were normalized to compare the depth changes at various healing times. The evolution of the normalized scratch depth was fitted with an exponential decay model, as described by eq 1 and illustrated in Figure S12, demonstrating that the underwater self-healing process also adheres to an exponential decay.[38]

$$d = d_\infty + (d_0 - d_\infty)e^{-t/\tau} \quad (1)$$

where τ is the time constant for the self-healing action, d_∞ is the residual depth, d represents the real-time scratch depth at different healing times, d_0 is the initial depth.

The glass transition temperature (T_g) is defined as the temperature at which molecular chains begin to mobilize, serving as a key parameter that indicate whether a material can underwater self-heal at conventional environment.[11,39] A lower T_g facilitated molecular chain mobility, enhancing the potential for underwater self-healing.[40−42] As shown in Figure S13, T_g increased with a higher SNOH content, primarily due to the presence of numerous aromatic rings in SNOH that restrict chain mobility. However, the T_g of DSFPUs remained below room temperature, which was advantageous for achieving underwater self-healing. To quantitatively assess the underwater self-healing capacity of the DSFPUs, we compared the

https://doi.org/10.1021/acs.macromol.4c03007
Macromolecules 2025, 58, 5019−5028

self-healing speeds at different temperatures by the following equation.

$$[\text{Self - healingspeed}] = [\text{notchsize}]/[\text{self - healingperiod}] \quad (2)$$

In this equation, the notch size refers to the thickness of the polyurethane film, measured at 0.4 mm, while the self-healing period represents the time taken for the notch to fully recover. The underwater self-healing images captured under polarized light microscopy at various temperatures are shown in Figure S14. The results in Figure 4d indicated that the underwater self-healing speed increased with increasing temperature, as higher temperatures accelerated dynamic bond exchange, thereby speeding up the self-healing process. Among them, DSFPU-3 exhibited the fastest underwater self-healing speed, reaching 33.33 μm/h at a conventional environment. At 60 °C, the self-healing speed increased further to 66.67 μm/h. However, DSFPU-1 only achieved underwater self-healing at temperatures above 50 °C due to its comparatively low dynamic bond content, which necessitated higher temperatures to promote dynamic bond exchange for underwater self-healing. Although DSFPU-4 had a higher dynamic bond content, its poor hydrophobicity allowed water molecules to interfere with some dynamic bond exchanges, thereby reducing the underwater self-healing speed. Consequently, DSFPU-3 achieved an optimal balance of hydrophobic and dynamic bond units, where the hydrophobic units shielded against water molecule interference and the dynamic bond units acted as the driving force for underwater self-healing, resulting in the outstanding self-healing performance. As shown in Figure 4e, DSFPU-3 was dyed with red and blue inks to create bone-shaped films of approximately 2 mm thickness, which were then cut in half and reassembled underwater in a conventional environment. After 12 h of underwater self-healing, the two bone-shaped films were firmly bonded together, capable of withstanding a 500 g weight without tearing (Movie S1).

2.5. Mechanistic Insights Into the Rapid Underwater Self-Healing. When DSFPUs sustain damage underwater, the alkyl side chains and fluorine groups repel water molecules, facilitating bond exchange between the tandem dynamic disulfide bonds and imine bonds, thereby achieving underwater self-healing (Figure 5a). The results in Figure 3b indicate that soaking in water did not affect the mechanical properties of DSFPU-3. We subjected the polyurethane samples to repair in a conventional underwater environment for different durations, and used the ratio of the strength after underwater self-healing to the original strength as the measure of underwater self-healing efficiency. As shown in Figure 5b, the mechanical strength of DSFPU-3 increased with a prolonged underwater self-healing time. After underwater self-healing for 12 h at a conventional environment, the self-healing efficiency reached 98% of the original strength. Furthermore, the self-healing performance was characterized through rheological oscillation strain tests conducted in water (Figure 5c). Under conventional conditions in water, after repeatedly reducing the strain from 1000 to 0.1%, both the storage modulus (G') and loss modulus (G'') of DSFPU-3 demonstrated good recovery. Repeated damage recovery tests indicated that DSFPU-3 could stably return to its original state without compromising its mechanical properties. At small strains, DSFPU-3 primarily exhibited elasticity, allowing it to quickly return to its original state. However, at large strains, the material became more flowable, and the exchange of tandem dynamic bonds played a crucial role.[20] This resulted in sliding and rearrangement of internal molecular chains, increasing viscosity and causing a transition from solid-like to liquid-like behavior. Additionally, the chain mobility of DSFPU-3 could be further elucidated through rheological measurements based on the time−temperature superposition principle. Clearly, both DSFPU-3 and DSFPU-C exhibited a crossover point at $G' = G''$ (Figure 5d,e), symbolizing the transition of the elastomer network from a physically cross-linked elastic state to a reversible, fluid-like state.[55] At low frequencies, the molecular chains have sufficient time to rearrange and respond to external stress, leading to a dominant viscous behavior. In contrast, at high frequencies, the polymer chains could not fully relax, causing the material to exhibit elastic behavior, as stress is stored rather than dissipated.[56] The reciprocal of the frequency at the crossover point was denoted as τ_c ($2\pi/\omega_c$), representing the ability of polymer chains to rearrange. The τ_c values for DSFPU-3 and DSFPU-C were 0.25 and 1.58 s, respectively, indicating that the rearrangement speed of the physical network in DSFPU-3 was relatively fast. This result also demonstrated that the tandem dynamic bonds could enhance the speed of underwater self-healing. Compared to previously reported polyurethanes and other polymers, our synthesized DSFPU-3 ranked among the best in terms of underwater healing time and efficiency (Figure 5f).[18,24,29,43−54] Additionally, we tested the biocompatibility of DSFPU-3. Figures S15 and S16 show that cells exhibited similar proliferation effects at various concentrations compared with the control culture medium. Culturing DSFPU-3 at a concentration of 10 cm^2/mL for 7 days produced proliferation results comparable to those of the control. Fluorescent staining results also indicated that DSFPU-3 and the control group have comparable proliferation rates, with almost no dead cells (Figure S17). These biological experiments demonstrated that DSFPU-3 possessed excellent biocompatibility, offering broad application prospects in implantable biomedical devices and biomedical scaffolds.

3. CONCLUSIONS

In summary, we successfully designed and synthesized a polyurethane (DSFPU-3) that achieves rapid underwater self-healing in a conventional environment, incorporating both dual hydrophobic units and tandem dynamic bonds. DSFPU-3 exhibited outstanding mechanical properties, including a tensile strength of 4.2 MPa, a strain of 534%, and a toughness value of 17.9 MJ m^{-3}. It maintained an elastic recovery rate of over 83%, even after five cycles of stretching at 100% strain. Additionally, DSFPU-3 demonstrated excellent water-proof properties, with a water contact angle of 99.3°. After 4 days of soaking in water, both the water contact angle and the mass remained unchanged. SEM and SAXS results further indicated stability in the microphase structure and micromorphology. The combination of hydrophobic alkyl side chains and fluorine groups provided dual protection, while the tandem disulfide and imine bonds acted as the driving force for self-healing under underwater conditions. In a conventional underwater environment, DSFPU-3 achieved complete self-healing within 12 h, with a speed of 33.33 μm/h, allowing it to support a weight of 500 g without breaking. The self-healing speed increased with temperature, reaching a self-healing efficiency of 98% in a conventional environment. Compared to DSFPU-C, rheological experiments confirmed that DSFPU-3 had a faster chain rearrangement capability, indicating that tandem dynamic bonds facilitated underwater self-healing. In addition,

https://doi.org/10.1021/acs.macromol.4c03007
Macromolecules 2025, 58, 5019−5028

DSFPU-3 demonstrated biocompatibility, highlighting its potential for broad applications in implantable medical devices. The strategic introduction and optimization of dual hydrophobic units and tandem dynamic bonds are crucial for enhancing the efficiency and speed of underwater self-healing, surpassing previous outcomes. This approach offers a novel method for fabricating underwater self-healing polymers.

4. EXPERIMENTAL SECTION

4.1. Synthesis of Chain Extender (SNOH) With Tandem Dynamic Bonds. 4-Aminodiphenyl disulfide (4.96 g, 0.02 mol) and *p*-methyl benzaldehyde (4.88 g, 0.04 mol) were dissolved in a flask containing 150 mL of ethanol. The mixture was then heated and stirred at 50 °C for 20 min, during which the solution gradually became transparent. Heating and stirring were continued at 50 °C for an additional 2 h, resulting in the precipitation of a large amount of light yellow powder. The precipitate could be collected by vacuum filtration and dried to obtain the final product, named SNOH, in a yield of 83.2%. The synthesis route and the ^{1}H NMR spectrum of SNOH are shown in Figure S18. The synthesis route for DPMI and DPBT aligned with the aforementioned methods, and the ^{1}H NMR spectrum is presented in Figures S19 and S20.

4.2. Synthesis and Purification of Poly(δ-dcanolactone) Diols (PDG). The poly(δ-decalactone) diols were synthesized via ring-opening polymerization as follows. In a glovebox filled with 99.999% Ar, a mixture of δ-decanolactone (DG, 16 g), 1,5,7-triazabicyclo[4.4.0]dec-5-ene (TBD, 0.20 g), and 1,4-benzenedimethanol (0.36 g) was added to a 50 mL stand-up flask equipped with a magnetic stir bar. The flask was sealed, removed from the glovebox, and placed on a magnetic stir plate at room temperature for 24 h. The mixture was then extracted in 500 mL of acetonitrile. Since the DG monomer was soluble in acetonitrile while PDG was not, DG was removed through basic extraction, which also eliminated TBD. This approach facilitated the isolation of pure PDG. The ^{1}H NMR spectrum of PDG, shown in Figure S21, confirmed the purity of PDG.

4.3. Synthesis of Underwater Polyurethane (DSFPUs). The following illustrates a specific example of the general procedure used to synthesize polyurethane. In a glovebox filled with 99.999% Ar, poly(δ-decalactone) diols (PDG, 10.2 g), FOH (1.7 g), SNOH (1.7 g), IPDI (3.1 g), and DBTDL (0.2 g) were mixed in a dried three-neck reactor equipped with a mechanical stirrer. DMF (13.0 g) was added to dissolve the mixture. The three-neck reactor was then sealed with a rubber septum, removed from the glovebox, and heated in an oil bath at 80 °C for 6 h. The stoichiometric ratio of [NCO]/[OH] was maintained as being equivalent. The resulting DSFPUs were precipitated in excess water and washed several times. The weight percentage ratios of [FOH]/[SNOH] were varied as follows: 3.4/0 (DSFPU-0), 2.55/0.85(DSFPU-1), 1.7/1.7 (DSFPU-2), 0.85/2.55 (DSFPU-3), and 0/3.4 (DSFPU-4). The contents and components used in the synthesis of DSFPUs are detailed in Table S1. Figure S22 shows the synthesis route. The synthesis method for DSFPU-C followed the same procedure as above, except that SNOH was replaced with HPS. The ^{1}H NMR spectra are shown in Figures S23 and S24.

■ ASSOCIATED CONTENT

Supporting Information

The Supporting Information is available free of charge at https://pubs.acs.org/doi/10.1021/acs.macromol.4c03007.

Materials, characterizations, cell viability test, time-of-flight mass spectra, ^{1}H NMR spectra, synthetic route, TGA curves and DTGA curves, the toughness of DSFPUs, changes in water contact angle and weight of DSFPUs after soaking for 4 days, DSC curves, optical microscope images, and fluorescent images of cells (PDF)

■ AUTHOR INFORMATION

Corresponding Authors

Jing Chen − *Key Laboratory of Bio-based Polymeric Materials Technology and Application of Zhejiang Province, Ningbo Institute of Materials Technology and Engineering, Chinese Academy of Sciences, Ningbo 315201, P. R. China*; Email: chenjing@nimte.ac.cn

Wu Bin Ying − *School of Electrical Engineering (EE), Korea Advanced Institute of Science and Technology (KAIST), Daejeon 34141, Republic of Korea*; orcid.org/0000-0002-8768-7428; Email: yingwubin@kaist.ac.kr

Authors

Fenglong Li − *Key Laboratory of Bio-based Polymeric Materials Technology and Application of Zhejiang Province, Ningbo Institute of Materials Technology and Engineering, Chinese Academy of Sciences, Ningbo 315201, P. R. China*

Haofeng Qiu − *Laboratory of Advanced Theranostic Materials and Technology, Ningbo Institute of Materials Technology and Engineering, Chinese Academy of Sciences, Ningbo 315300, P. R. China*

Chao Chen − *Department of Chemical Engineering and Applied Chemistry, Chungnam National University, Daejeon 34134, Republic of Korea*

Xiaolin Wang − *Key Laboratory of Bio-based Polymeric Materials Technology and Application of Zhejiang Province, Ningbo Institute of Materials Technology and Engineering, Chinese Academy of Sciences, Ningbo 315201, P. R. China*

Minghui Cui − *Key Laboratory of Bio-based Polymeric Materials Technology and Application of Zhejiang Province, Ningbo Institute of Materials Technology and Engineering, Chinese Academy of Sciences, Ningbo 315201, P. R. China*

Shijie Qiu − *Department of Otorhinolaryngology Head and Neck Surgery, Ningbo Medical Center Lihuili Hospital, Ningbo 315041, P. R. China*; orcid.org/0000-0001-9417-165X

Kyung Jin Lee − *Department of Chemical Engineering and Applied Chemistry, Chungnam National University, Daejeon 34134, Republic of Korea*; orcid.org/0000-0002-6709-3235

Jin Zhu − *Key Laboratory of Bio-based Polymeric Materials Technology and Application of Zhejiang Province, Ningbo Institute of Materials Technology and Engineering, Chinese Academy of Sciences, Ningbo 315201, P. R. China*

Complete contact information is available at: https://pubs.acs.org/10.1021/acs.macromol.4c03007

Notes

The authors declare no competing financial interest.

■ ACKNOWLEDGMENTS

This work was supported by the National Natural Science Foundation of China (U21B2093 and U23A20691), the S&T Innovation 2025 Major Special Program of Ningbo (2022Z139), and the Brain Pool program (RS-2023-00222619) funded by the Ministry of Science and ICT through the National Research Foundation of Korea.

■ REFERENCES

(1) Cerdan, K.; Thys, M.; Costa Cornellà, A.; Demir, F.; Norvez, S.; Vendamme, R.; Van den Brande, N.; Van Puyvelde, P.; Brancart, J. Sustainability of self-healing polymers: A holistic perspective towards

circularity in polymer networks. *Prog. Polym. Sci.* **2024**, *152*, No. 101816.
(2) Liu, C.; Kelley, S. O.; Wang, Z. Self-healing materials for bioelectronic devices. *Adv. Mater.* **2024**, *36* (35), No. 2401219.
(3) Chen, W. C.; Wang, R. C.; Yu, S. K.; Chen, J. L.; Kao, Y. H.; Wang, T. Y.; Chang, P. Y.; Sheu, H. S.; Chen, S. C.; Liu, W. R.; Yang, T. I.; Wu, H. C. Self-healable spider dragline silk materials. *Adv. Funct. Mater.* **2023**, *33* (44), No. 2303571.
(4) Xiong, H.; Wu, H.; Zhang, J.; Huang, S.; Gu, S.; Hou, Y.; Wu, Q.; Wu, J. Healable and recyclable polyurethane with natural-rubber-like resilience via π-type tweezer structure stabilizing dynamical hard domains. *Macromolecules* **2023**, *56* (21), 8581−8591.
(5) Jin, Q.; Du, R.; Tang, H.; Zhao, Y.; Peng, W.; Li, Y.; Zhang, J.; Zhu, T.; Huang, X.; Kong, D.; He, Y.; Bao, T.; Kong, D.; Wang, X.; Wang, R.; Zhang, Q.; Jia, X. Quadruple h-bonding and polyrotaxanes dual cross-linking supramolecular elastomer for high toughness and self-healing conductors. *Angew. Chem., Int. Ed. Engl.* **2023**, *62* (26), No. 202305282.
(6) Ren, Y.; Dong, X. Dynamic polymeric materials via hydrogen-bond cross-linking: Effect of multiple network topologies. *Prog. Polym. Sci.* **2024**, *158*, No. 101890.
(7) Chen, C.; Yu, Z.; Tian, Y.; Li, F.; Kong, Z.; Ran, X.; Wu, X.; Lee, K. J.; Kim, D. H.; Lee, J. Y.; Zhu, J.; Ying, W. B. Transmembrane inspired mechano-responsive elastomers with synergized traction-assisted healing and dual-channel sensing. *Adv. Funct. Mater.* **2024**, *34* (37), No. 2402380.
(8) Ying, W. B.; Wang, G.; Kong, Z.; Yao, C. K.; Wang, Y.; Hu, H.; Li, F.; Chen, C.; Tian, Y.; Zhang, J.; Zhang, R.; Zhu, J. A biologically muscle-inspired polyurethane with super-tough, thermal reparable and self-healing capabilities for stretchable electronics. *Adv. Funct. Mater.* **2021**, *31* (10), No. 2009869.
(9) Raut, S. K.; Asha, A. B.; Singha, N. K.; Narain, R. Ultrafast derived self-healable, reprocessable polyurethane elastomer based on dynamic "electrophilic substitution (ES)-click" chemistry. *Macromolecules* **2022**, *55* (23), 10264−10275.
(10) Li, C. H.; Zuo, J. L. Self-healing polymers based on coordination Bonds. *Adv. Mater.* **2020**, *32* (27), No. e1903762.
(11) Li, F.; Xu, Z.; Hu, H.; Kong, Z.; Chen, C.; Tian, Y.; Zhang, W.; Bin Ying, W.; Zhang, R.; Zhu, J. A polyurethane integrating self-healing, anti-aging and controlled degradation for durable and eco-friendly E-skin. *Chem. Eng. J.* **2021**, *410*, No. 128363.
(12) Jung, J.; Lee, S.; Kim, H.; Lee, W.; Chong, J.; You, I.; Kang, J. Self-healing electronic skin with high fracture strength and toughness. *Nat. Commun.* **2024**, *15* (1), 9763.
(13) Feng, H.; Wang, S.; Lim, J. Y. C.; Li, B.; Rusli, W.; Liu, F.; Hadjichristidis, N.; Li, Z.; Zhu, J. Catalyst-free alpha-acetyl cinnamate/acetoacetate exchange to enable high creep-resistant vitrimers. *Angew. Chem., Int. Ed. Engl.* **2024**, *63* (20), No. e202400955.
(14) Wang, S.; Feng, H.; Lim, J. Y. C.; Li, K.; Li, B.; Mah, J. J. Q.; Xing, Z.; Zhu, J.; Loh, X. J.; Li, Z. Recyclable, malleable, and strong thermosets enabled by Knoevenagel adducts. *J. Am. Chem. Soc.* **2024**, *146* (14), 9920−9927.
(15) Chen, Y.; Chen, B.; Torkelson, J. M. Biobased, reprocessable non-isocyanate polythiourethane networks with thionourethane and disulfide cross-links: comparison with polyhydroxyurethane network analogues. *Macromolecules* **2023**, *56* (10), 3687−3702.
(16) Chen, S.; Ding, J.; Zhao, Y.; Yuan, A.; Liao, Y.; Chen, X.; Lei, Y.; Jiang, L.; Lei, J.; Fu, X. Design of robust and recyclable covalent elastomeric networks through dynamic enamine−urea bonds. *Macromolecules* **2024**, *57*, 8813−8825.
(17) Yimyai, T.; Crespy, D.; Pena-Francesch, A. Self-healing photochromic elastomer composites for wearable UV-sensors. *Adv. Funct. Mater.* **2023**, *33* (20), No. 2213717.
(18) Xu, L.; Huang, Z.; Deng, Z.; Du, Z.; Sun, T. L.; Guo, Z. H.; Yue, K. A transparent, highly stretchable, solvent-resistant, recyclable multifunctional ionogel with underwater self-Healing and adhesion for reliable strain sensors. *Adv. Mater.* **2021**, *33* (51), No. 2105306.
(19) Yao, H.; Liu, T.; Jia, Y.; Du, Y.; Yao, B.; Xu, J.; Fu, J. Water-insensitive self-healing materials: from network structure design to advanced soft electronics. *Adv. Funct. Mater.* **2023**, *33* (48), No. 2307455.
(20) Kong, Z.; Boahen, E. K.; Kim, D. J.; Li, F.; Kim, J. S.; Kweon, H.; Kim, S. Y.; Choi, H.; Zhu, J.; Bin Ying, W.; Kim, D. H. Ultrafast underwater self-healing piezo-ionic elastomer via dynamic hydrophobic-hydrolytic domains. *Nat. Commun.* **2024**, *15* (1), 2129.
(21) Sedo, J.; Saiz-Poseu, J.; Busque, F.; Ruiz-Molina, D. Catechol-based biomimetic functional materials. *Adv. Mater.* **2013**, *25* (5), 653−701.
(22) Song, K.; Ye, W.; Gao, X.; Fang, H.; Zhang, Y.; Zhang, Q.; Li, X.; Yang, S.; Wei, H.; Ding, Y. Synergy between dynamic covalent boronic ester and boron-nitrogen coordination: strategy for self-healing polyurethane elastomers at room temperature with unprecedented mechanical properties. *Mater. Horiz.* **2021**, *8* (1), 216−223.
(23) Yin, H.; Liu, F.; Abdiryim, T.; Liu, X. Self-healing hydrogels: from synthesis to multiple applications. *ACS Materials Lett.* **2023**, *5* (7), 1787−1830.
(24) Liu, M.; Liu, P.; Lu, G.; Xu, Z.; Yao, X. Multiphase-assembly of siloxane oligomers with improved mechanical strength and water-enhanced healing. *Angew. Chem., Int. Ed. Engl.* **2018**, *57* (35), 11242−11246.
(25) Liu, T.; Li, C.; Yao, H.; Sun, F.; Wang, L.; Yao, B.; Xu, J.; Fu, J. Extremely strengthening fatigue resistance, elastic restorability and thermodynamic stability of a soft transparent self-healing network based on a dynamic molecular confinement-induced bioinspired nanostructure. *Mater. Horiz.* **2023**, *10* (8), 2968−2979.
(26) Ying, W. B.; Yu, Z.; Kim, D. H.; Lee, K. J.; Hu, H.; Liu, Y.; Kong, Z.; Wang, K.; Shang, J.; Zhang, R.; Zhu, J.; Li, R. W. Waterproof, highly tough, and fast self-healing polyurethane for durable electronic skin. *ACS Appl. Mater. Interfaces* **2020**, *12* (9), 11072−11083.
(27) Cheng, Z.; Feng, W.; Zhang, Y.; Sun, L.; Liu, Y.; Chen, L.; Wang, C. A highly robust amphibious soft robot with imperceptibility based on a water-stable and self-healing ionic conductor. *Adv. Mater.* **2023**, *35* (28), No. 2301005.
(28) Kang, J.; Son, D.; Wang, G. N.; Liu, Y.; Lopez, J.; Kim, Y.; Oh, J. Y.; Katsumata, T.; Mun, J.; Lee, Y.; Jin, L.; Tok, J. B.; Bao, Z. Tough and water-insensitive self-healing elastomer for robust electronic skin. *Adv. Mater.* **2018**, *30* (13), No. e1706846.
(29) Khatib, M.; Zohar, O.; Saliba, W.; Srebnik, S.; Haick, H. Highly efficient and water-insensitive self-healing elastomer for wet and underwater electronics. *Adv. Funct. Mater.* **2020**, *30* (22), No. 1910196.
(30) Guo, Q.; Huang, B.; Lu, C.; Zhou, T.; Su, G.; Jia, L.; Zhang, X. A cephalopod-inspired mechanoluminescence material with skin-like self-healing and sensing properties. *Mater. Horiz.* **2019**, *6* (5), 996−1004.
(31) Pena-Francesch, A.; Jung, H.; Demirel, M. C.; Sitti, M. Biosynthetic self-healing materials for soft machines. *Nat. Mater.* **2020**, *19* (11), 1230−1235.
(32) Hernroth, B.; Farahani, F.; Brunborg, G.; Dupont, S.; Dejmek, A.; Skold, H. N. Possibility of mixed progenitor cells in sea star arm regeneration. *J. Exp. Zool., Part B* **2010**, *314* (6), 457−468.
(33) Franco, C. F.; Santos, R.; Coelho, A. V. Exploring the proteome of an echinoderm nervous system: 2-DE of the sea star radial nerve cord and the synaptosomal membranes subproteome. *Proteomics* **2011**, *11* (7), 1359−1364.
(34) Kim, C. H.; Go, H. J.; Oh, H. Y.; Park, J. B.; Lee, T. K.; Seo, J. K.; Elphick, M. R.; Park, N. G. Identification of a novel antimicrobial peptide from the sea star Patiria pectinifera. *Dev. Comp. Immunol.* **2018**, *86*, 203−213.
(35) Xu, X.; Ma, S.; Feng, H.; Qiu, J.; Wang, S.; Yu, Z.; Zhu, J. Dissociate transfer exchange of tandem dynamic bonds endows covalent adaptable networks with fast reprocessability and high performance. *Polym. Chem.* **2021**, *12* (36), 5217−5228.

https://doi.org/10.1021/acs.macromol.4c03007
Macromolecules 2025, 58, 5019−5028

(36) Xu, X.; Wu, J.; Li, M.; Wang, S.; Feng, H.; Wang, B.; Hu, K.; Zhang, C.; Zhu, J.; Ma, S. Synergistic catalytic effect of triple dynamic bonds for fast-reprocessing and high-performance cross-linked polymers. *Polym. Chem.* **2023**, *14* (4), 523−532.
(37) Li, F.; Kong, Z.; Wang, X.; Wang, G.; Chen, C.; Tian, Y.; Lyu, Z.; Lee, K. J.; Kim, D. H.; Lee, J.-Y.; Zhu, J.; Ying, W. B. A bio-based, sweat-resistant and markedly sensitive iontronic skin for advancing central sleep apnea monitoring. *Chem. Eng. J.* **2024**, *487*, No. 150541.
(38) Brancart, J.; Verhelle, R.; Mangialetto, J.; Van Assche, G. Coupling the mcroscopic haling behaviour of coatings to the thermoreversible Diels-Alder network formation. *Coatings* **2019**, *9* (1), 13.
(39) Zhang, L.; Liu, Z.; Wu, X.; Guan, Q.; Chen, S.; Sun, L.; Guo, Y.; Wang, S.; Song, J.; Jeffries, E. M.; He, C.; Qing, F. L.; Bao, X.; You, Z. A highly efficient self-healing elastomer with unprecedented mechanical properties. *Adv. Mater.* **2019**, *31* (23), No. 1901402.
(40) Chen, C.; Ying, W. B.; Li, J.; Kong, Z.; Li, F.; Hu, H.; Tian, Y.; Kim, D. H.; Zhang, R.; Zhu, J. A self-healing and ionic liquid affiliative polyurethane toward a Piezo 2 protein inspired ionic skin. *Adv. Funct. Mater.* **2021**, *32* (4), No. 2106341.
(41) Li, F.; Wang, X.; Zuo, J.; Chen, C.; Chen, J.; Zhu, J.; Ying, W. B. Oxime-urethane-based self-healing polyurethane for achieving complex structures via 3D printing. *ACS Appl. Polym. Mater.* **2024**, *6* (7), 4070−4077.
(42) Ying, W. B.; Liu, H.; Gao, P.; Kong, Z.; Hu, H.; Wang, K.; Shen, A.; Jin, Z.; Zheng, L.; Guo, H.; Zhang, R.; Zhu, J. An anti-stress relaxation, anti-fatigue, mildew proof and self-healing poly-(thiourethane-urethane) for durably stretchable electronics. *Chem. Eng. J.* **2021**, *420*, No. 127691.
(43) Zhang, Y.; Li, M.; Qin, B.; Chen, L.; Liu, Y.; Zhang, X.; Wang, C. Highly transparent, underwater self-healing, and ionic conductive elastomer based on multivalent ion−dipole interactions. *Chem. Mater.* **2020**, *32* (15), 6310−6317.
(44) Xia, N. N.; Rong, M. Z.; Zhang, M. Q. Stabilization of catechol−boronic ester bonds for underwater self-healing and recycling of lipophilic bulk polymer in wider pH range. *J. Mater. Chem. A* **2016**, *4* (37), 14122−14131.
(45) Wang, N.; Zhang, L.; Liu, J.; Li, C. An integrally underwater self-healable droplet-based triboelectric nanogenerator. *J. Mater. Chem. A* **2022**, *10* (38), 20509−20516.
(46) Li, J.; Ejima, H.; Yoshie, N. Seawater-assisted self-healing of catechol polymers via hydrogen bonding and coordination interactions. *ACS Appl. Mater. Interfaces* **2016**, *8* (29), 19047−19053.
(47) Kim, C.; Ejima, H.; Yoshie, N. Non-swellable self-healing polymer with long-term stability under seawater. *RSC Adv.* **2017**, *7* (31), 19288−19295.
(48) Cao, Y.; Wu, H.; Allec, S. I.; Wong, B. M.; Nguyen, D. S.; Wang, C. A Highly stretchy, transparent elastomer with the capability to automatically self-heal underwater. *Adv. Mater.* **2018**, *30* (49), No. 1804602.
(49) Cao, Y.; Tan, Y. J.; Li, S.; Lee, W. W.; Guo, H.; Cai, Y.; Wang, C.; Tee, B. C. K. Self-healing electronic skins for aquatic environments. *Nat. Electron.* **2019**, *2* (2), 75−82.
(50) Xu, J.; Wang, H.; Wen, X.; Wang, S.; Wang, H. Mechanically strong, wet adhesive, and self-healing polyurethane ionogel enhanced with a semi-interpenetrating network for underwater motion detection. *ACS Appl. Mater. Interfaces* **2022**, *14* (48), 54203−54214.
(51) Xia, N. N.; Xiong, X. M.; Rong, M. Z.; Zhang, M. Q.; Kong, F. Self-healing of polymer in acidic water toward strength restoration through the synergistic effect of hydrophilic and hydrophobic interactions. *ACS Appl. Mater. Interfaces* **2017**, *9* (42), 37300−37309.
(52) Peng, W. L.; Zhang, Z. P.; Rong, M. Z.; Zhang, M. Q. Reversibly interlocked macromolecule networks with enhanced mechanical properties and wide pH range of underwater self-healability. *ACS Appl. Mater. Interfaces* **2020**, *12* (24), 27614−27624.
(53) Liu, Y.; Zheng, J.; Zhang, X.; Du, Y.; Yu, G.; Li, K.; Jia, Y.; Zhang, Y. Bioinspired modified graphene oxide/polyurethane composites with rapid self-healing performance and excellent mechanical properties. *RSC Adv.* **2021**, *11* (24), 14665−14677.
(54) He, C. L.; Liang, F. C.; Veeramuthu, L.; Cho, C. J.; Benas, J. S.; Tzeng, Y. R.; Tseng, Y. L.; Chen, W. C.; Rwei, A.; Kuo, C. C. Super tough and spontaneous water-assisted autonomous self-healing elastomer for underwater wearable electronics. *Adv. Sci.* **2021**, *8* (21), No. e2102275.
(55) Liu, X.; Liu, X.; Li, W.; Ru, Y.; Li, Y.; Sun, A.; Wei, L. Engineered self-healable elastomer with giant strength and toughness via phase regulation and mechano-responsive self-reinforcing. *Chem. Eng. J.* **2021**, *410*, No. 128300.
(56) Sun, F.; Zhang, J.; Liu, T.; Yao, H.; Wang, L.; Meng, H.; Gao, Y.; Cao, Y.; Yao, B.; Xu, J.; Fu, J. A versatile microporous design toward toughened yet softened self-healing materials. *Adv. Mater.* **2024**, *36* (50), No. e2410650.

https://doi.org/10.1021/acs.macromol.4c03007
Macromolecules 2025, 58, 5019−5028